Electrochimica Acta 497 (2024) 144582

Contents lists available at ScienceDirect

Electrochimica Acta

journal homepage: www.journals.elsevier.com/electrochimica-acta

Impedance spectroscopy using microscopic reference electrodes to analyze different rate-determining steps in aqueous dye-sensitized solar cells using nitroxide radicals as redox mediators

Daniel Holzhacker, Andreas Ringleb, Derck Schlettwein *

Institut für Angewandte Physik, Justus-Liebig-Universität Giessen, Heinrich-Buff-Ring 16, Giessen, Hesse 35392, Germany

ARTICLE INFO

Keywords:
Photoelectrochemistry
Dye-Sensitized Solar Cell (DSSC)
Electrode kinetics
Aqueous redox electrolyte
Mediator regeneration

ABSTRACT

For new components in dye-sensitized solar cells (DSSCs), identification and quantification of rate-limiting steps is needed to evaluate their applicability. This is particularly important if fundamental changes are studied. In this work, the use of a micro-reference electrode in DSSCs is proposed to increase the significance of electrochemical impedance spectroscopy. The recombination of charge carriers at the photoanode and the regeneration of redox mediators at the counter electrode, which typically occur on similar timescales, could be studied separately but simultaneously in cells under operating conditions. This is particularly useful in the study of water-based DSSCs. Here, cells with 2,2,6,6-Tetramethylpiperidinoxyl (TEMPO) or 4-Hydroxy-TEMPO (OH-TEMPO) as redox mediators using additives like 1-Methylbenzimidazole (MBI) are discussed. It was revealed that the charge transfer resistance (R_{CE}) for the reduction of the oxidized redox mediator at the counter electrode (CE) limits the fill factor (*FF*) of such DSSCs. TEMPO/MBI electrolytes yielded low R_{CE} and high *FF*, whereas OH-TEMPO in otherwise identical cells resulted in large R_{CE}, low *FF*, and low conversion efficiencies. This indicates that the interface between the CE and the electrolyte significantly influences the DSSC performance of these cells and strongly depends on the electrolyte composition. Important optimization strategies could be discussed based on the present results.

1. Introduction

Dye-sensitized solar cells (DSSCs) serve as an alternative concept for the photovoltaic (PV) conversion of light into electricity. Despite their low power conversion efficiency (*PCE*) under standard AM1.5 conditions, DSSCs are of technical interest due to their low energy payback times, low toxicity, and versatile applications in, e.g., building-integrated or indoor PV [1–3]. Referring to the latter, DSSCs provided good *PCE*s in part even out-performing established Si-based cells [4].

In an ongoing attempt to increase the sustainability of DSSCs further, the substitution of the commonly used solvent acetonitrile with water became a central aspect of research [5–7]. Also, the most efficient redox mediators, i.e. iodine (I^-/I_3^-) or cobalt complexes such as $Co^{III/II}$(6-(1H-pyrazol-1-yl)−2,20-bipyridine) ($Co(bpy\text{-}pz)^{3+/2+}$), are problematic due to the disadvantageous optical properties and low solubility of iodine [8,9] as well as the carcinogenicity of cobalt [10].

As an alternative, aqueous solutions of the nitroxide-radical 2,2,6,6-tretramethylpiperidinoxyl (TEMPO) have been suggested, owing to rapid one-electron transfer kinetics and a highly positive redox potential $E_{redox} = 0.71$ V vs. NHE [11] (compared to 0.35 V for I^-/I_3^- [9] or 0.60 V for $Co(bpy\text{-}pz)^{3+/2+}$ [12]). Aqueous TEMPO-based DSSCs have been reported and already achieved a *PCE* of 4.1 % with a high open-circuit voltage $V_{oc} = 0.955$ V, short-circuit photocurrent density $j_{sc} = 5.78$ mA cm^{-2}, fill factor $FF = 0.75$, using a concentration $C_{TEMPO} = 0.15$ M [11]. However, the low solubility of TEMPO in water < 0.15 M limits the j_{sc} and, hence, *PCE*. In order to increase the j_{sc}, higher concentrations of the redox mediator (C_{redox}) are desired since j_{sc} can in first approximation be assumed to be proportional to C_{redox}.

The hydrophilic TEMPO-derivative 4-Hydroxy-TEMPO (OH-TEMPO) is a promising candidate due to its cost-effective synthesis from abundant chemicals (acetone and ammonia), high solubility in water ($C_{OH\text{-}TEMPO,\ max} > 2$ M), and $E_{redox} = 0.81$ V vs. NHE, even more positive than that of TEMPO [13]. However, a successful example for the application of OH-TEMPO in aqueous DSSCs yielded *PCE* = 2.1 % (j_{sc} = 4.5 mA cm^{-2}, $V_{oc} = 0.69$ V, $FF = 0.64$, $C_{OH\text{-}TEMPO} = 1.0$ M), while a rather complex counter electrode (CE) of Nafion-coated Pt had to be used [14].

* Corresponding author.
E-mail address: schlettwein@uni-giessen.de (D. Schlettwein).

https://doi.org/10.1016/j.electacta.2024.144582
Received 5 February 2024; Received in revised form 3 May 2024; Accepted 9 June 2024
Available online 10 June 2024

It is, thereby, indicated that an optimized interaction of OH-TEMPO with the CE of the DSSC is of great importance to fully exploit its potential as redox mediator and should be studied in detail. However, in the common DSSC architecture consisting of the sensitized photoanode (working electrode, WE) and CE, the CE properties have to be extracted either from the impedance data of a full cell, in which different processes are typically found superimposed at similar frequencies, or from separately built model systems, e.g., symmetrical cells with another CE instead of the photoanode. The former approach typically does not allow a reliable characterization of the counter electrode kinetics, while the latter approach does not allow simultaneous characterization of the reactions at the WE, which is decisive in DSSCs. Further, unknown side products from the illuminated photoanode might as well interact with the CE and cannot be studied in such symmetrical cells.

Similar problems were also faced in lithium-ion battery [15–19] and solid-oxide fuel cell [20–22] research, where the application of an additional microscopic quasi-reference electrode (μRE) receives ongoing attention to separately and simultaneously determine the impedance of anodes and cathodes under operating conditions, both individually referred to the common μRE in the cells.

Here, we used a similar approach to introduce appropriate μREs into DSSCs. Previous attempts to include a macroscopic reference electrode in DSSCs significantly altered the cell architecture and, hence, negatively affected important cell properties and, e.g., added an additional diffusion resistance due to an unrealistically large electrode distance [23,24]. In the present work, by using a micrometer-sized metal wire as a μRE, the electrode kinetics at both WE and CE of DSSCs could be studied *in operando* and, hence, details of the rate-limiting steps in aqueous DSSCs could be revealed.

2. Experimental

2.1. Cell preparation

Aqueous DSSCs were prepared by sandwiching a TiO_2 photoanode and a poly(3,4-ethylenedioxythiophene) (PEDOT) counter electrode with a melting polymer foil (Meltonix, thickness = 25 μm, *Solaronix*). The photoanodes consisted of a spin-coated blocking layer (Ti-Nanoxide BL/SC, *Solaronix*, 50 μL, 3000 rpm for 30 s) and a circular (diameter d = 6 mm), 2 – 4 μm thick screen-printed layer of porous TiO_2 (18 NR-T paste, *Greatcell Solar*) on FTO (KV-FTO-R15, *Kaivo*). The TiO_2 films were annealed at 500 °C. After immersion in a 40 mM aqueous $TiCl_4$ (*TCI*) solution for 30 min at 70 °C and subsequent firing at 500 °C for 1 h [25], the porous TiO_2 was sensitized in a 0.2 mM dye solution of Y123 (*Dyenamo*) in ethanol overnight. The counter electrodes consisted of electrodeposited PEDOT on FTO substrates with two predrilled holes for the injection of the electrolyte. PEDOT was electrodeposited from an aqueous solution of 0.01 M 3,4-ethylenedioxythiophene (*TCI*) and 0.1 M sodium dodecyl sulfate (*Roth*) at a current density of 0.2 mA cm^{-2} for 100 s. In the case of three-electrode DSSCs, two layers of the melting foil sandwiching a thin platinum wire (d = 25 μm) were placed between the WE and CE with no additional measures needed to prevent short-circuits. Symmetric cells consisted of two PEDOT-coated substrates (one with holes for electrolyte injection, one without holes), connected by one layer of melting foil.

The TEMPO electrolyte solutions consisted of 0.1 M TEMPO (*Aldrich*), 0.05 M $TEMPOBF_4$, and 0.02 M $LiClO_4$ (*Roth*) in deionized water (σ = 0.85 μS cm^{-1}). For OH-TEMPO electrolytes, OH-TEMPO (*TCI*) and OH-$TEMPOBF_4$ were used instead of TEMPO. $TEMPOBF_4$ and OH-$TEMPOBF_4$ were synthesized [26] from TEMPO and OH-TEMPO, respectively, in the presence of HBF_4 and NaOCl solution (*Roth*, 12 % Cl) and recrystallized from water and the products yielded the expected redox potentials [11,13] as confirmed by cyclic voltammetry (Fig. S1). To some electrolyte solutions, 0.2 M 1-methylbenzimidazole (MBI, *Aldrich*) or 0.05 M *tert*-butylpyridine (TBP, *Aldrich*) were added. Further, a 1.0 M OH-TEMPO (including 0.5 M OH-$TEMPOBF_4$ and 0.02 M $LiClO_4$) electrolyte was used. All chemicals were used without further purification. All filling holes in the CEs were sealed with melting foil and glass cover slips.

2.2. Characterization

Electrochemical impedance spectroscopy (EIS) and measurements of the current density (j) depending on the applied potential difference (V_{appl}) on DSSCs were carried out using a *BioLogic* SP-50e potentiostat under AM1.5 G illumination, realized with a Xenon lamp (*LOT Oriel*) controlled by a calibrated silicon diode (*EKO Instruments*). EIS experiments were performed at open-circuit with a modulation amplitude of 10 mV between CE and WE in a frequency (f) range of $10^5 – 10^{-1}$ Hz. To test for limitations by the reactions at the CE for a given electrolyte composition, the dependence of j on V_{appl} was measured for symmetrical cells in cyclic potential sweeps with the SP-50e in the dark. For all j-V_{appl} curves, a scan rate of 50 mV s^{-1} was used. EIS data were fitted with the help of the software RelaxIS (*rhd instruments*). Fig. 1 shows the architecture of a μRE-DSSC including the equivalent circuit used in this work. The transmission line model was chosen as established in the literature on DSSCs [27]. To describe parallel circuits of a resistor (R) and a constant phase element (shown as << in Fig. 1), i.e., to model charge transfer at the solid | liquid interfaces, Zarc elements were used [28].

3. Results and discussion

3.1. Photovoltaic cell characteristics

Fig. 2a shows j-V curves of DSSCs with differently composed electrolyte solutions. The 0.1 M TEMPO/MBI cell achieved a power conversion efficiency (*PCE*) of 2.98 % owing to a high V_{oc} and *FF* but small j_{sc} limited by the low achievable concentration of the redox mediator (Table 1). Substituting TEMPO with OH-TEMPO at the same concentration yielded a higher j_{sc} and V_{oc}, showing the attractive characteristics of this redox mediator. However, a significantly smaller *FF* was reached, leading to a poor *PCE*. Trying to overcome part of the problem by replacement of MBI by a different organic additive (4-*tert*-butylpyridine, TBP) resulted in an even inferior DSSC. An identically low *FF* and even smaller j_{sc} and V_{oc} were measured. Not using additives at all yielded a satisfying *FF*, similar to 0.1 M TEMPO/MBI, but j_{sc} and V_{oc} were considerably smaller, indicating very fast recombination at the photoanode, speaking in favor of a constructive role of MBI and TBP as additives to suppress recombination at the WE but, apparently, of a competing problematic role in other parts of the cell, decreasing the *FF*. Increasing the OH-TEMPO concentration to 1.0 M without additives resulted in a complete loss of the generated electrons, underlining the necessity to use additives to suppress recombination at the WE.

To elucidate the problems caused by the additives in the cells, the respective electrolyte | CE interfaces were studied by CV experiments in symmetric cells (Fig. 2b), in order to analyze the effects of different additives on the kinetics at the PEDOT counter electrodes. TEMPO/MBI electrolytes showed diffusion-limited, i.e., Ohmic behavior for small overpotentials and saturation at the diffusion-limited current density (j_{lim}).

In contrast, the corresponding OH-TEMPO/MBI electrolyte showed kinetically limited characteristics, i.e., overpotentials of > 0.4 V necessary to draw a significant current. This was also seen to a similar extent when using TBP. These additives were needed to achieve an appreciable V_{oc} at the photoanode (Fig. 2a), but obviously their (advantageous) activity was not just limited to the photoanode but also (disadvantageously) affected the cathode. In contrast, additive-free solutions of OH-TEMPO showed diffusion-limited characteristics, proving the responsibility of the organic additives for the observed kinetic limitation of the charge transfer reactions at PEDOT. Thus, the pure OH-TEMPO | PEDOT interface seems to be suitable for DSSCs, albeit the charge transfer resistance was slightly higher, and the diffusion-limited current

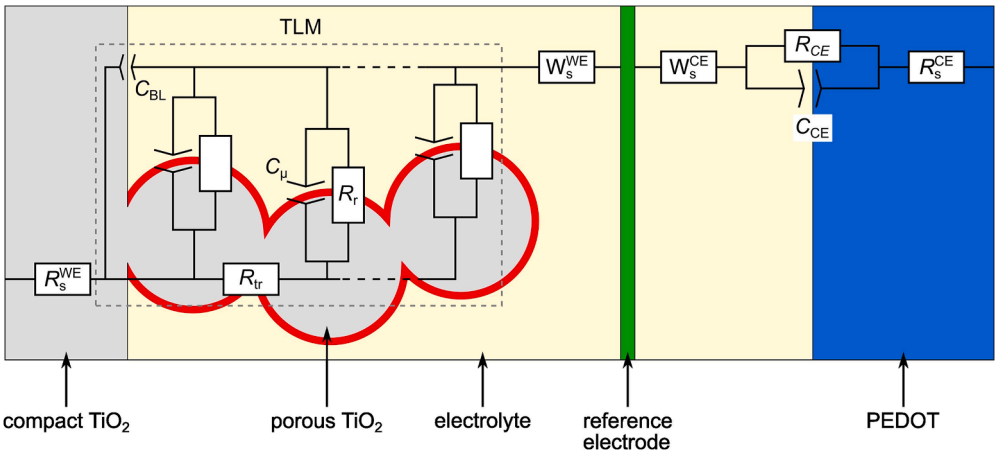

Fig. 1. Schematic representation of the equivalent circuit of a DSSC used to fit the data. The cell is divided into two half-cells by the reference electrode. The photoanode half-cell consists of a series resistance (R_s^{WE}), a transmission line model (TLM), and a Warburg-short element (W_s^{WE}) describing the ionic conductivity of the electrolyte. In the TLM, R_{tr} denotes the electrical transport resistance along the TiO_2 nanoparticles, R_r is the recombination resistance, C_μ is the chemical capacitance, and C_{BL} is the capacitance of the blocking layer | electrolyte interface. The counter electrode half-cell is composed of one Zarc element modeling the charge transfer at the electrolyte | PEDOT interface (R_{CE} and C_{CE}), a Warburg-short element (W_s^{CE}), and a series resistance (R_s^{CE}).

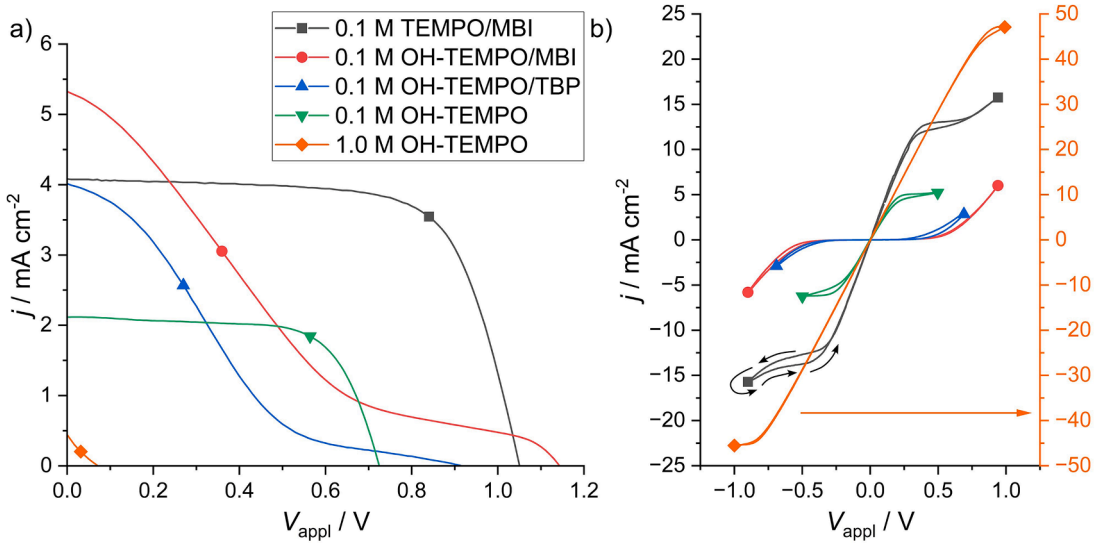

Fig. 2. *j-V* curves of TEMPO and OH-TEMPO electrolytes in (a) DSSCs (maximum power points marked by symbols) and (b) symmetric cells consisting of two PEDOT-substrates (vertex potentials marked by symbols, loop indicated by arrows on the 0.1 M TEMPO/MBI curve, right axis for 1.0 M OH-TEMPO only). Cyclic voltammograms of the redox mediators using a reference electrode are depicted in Fig. S1.

Table 1
Solar cell characteristics of DSSCs with different TEMPO- and OH-TEMPO-based electrolytes under AM1.5 illumination.

Redox-Mediator	Additive	j_{sc} / mA cm^{-2}	V_{oc} / V	*FF*	*PCE* / %
0.1 M TEMPO	0.20 M MBI	4.07	1.05	0.70	2.98
0.1 M OH-TEMPO	0.20 M MBI	5.33	1.14	0.18	1.10
0.1 M OH-TEMPO	0.05 M TBP	4.01	0.92	0.19	0.69
0.1 M OH-TEMPO	None	2.12	0.73	0.64	1.04
1.0 M OH-TEMPO	None	0.44	0.07	0.20	0.01

density was slightly lower ($R_{CV,\ OH\text{-}TEMPO} = 40.0\ \Omega$, $j_{lim,\ OH\text{-}TEMPO} = 6$ mA cm^{-2}) than for the reference 0.1 M TEMPO/MBI electrolyte ($R_{CV,\ TEMPO} = 21.6\ \Omega$, $j_{lim,\ TEMPO} = 14$ mA cm^{-2}). The influence of additives, however, inevitable for well-performing photoanodes, deserves special attention on the OH-TEMPO | PEDOT interface.

3.2. Establishing μRE-EIS in DSSCs using TEMPO as redox mediator

To precisely investigate the CE kinetics in DSSCs under operating conditions, impedance measurements assisted by the use of micro-reference electrodes were performed, in which the photoanode (WE) vs. μRE and the PEDOT counter electrode (CE) vs. μRE impedance contributions were simultaneously obtained but could be evaluated separately. To establish the validity of such experiments, the influence of the adjusted DSSC architecture was studied. Therefore, DSSC in three different architectures (concerning the spatial separation of WE and CE) were compared:

Type A: one melting foil spacer (25 μm electrode spacing, regular arrangement in DSSCs),
Type B: two melting foil spacers (50 μm electrode spacing to test for the impact of larger distance),
Type C: two melting foil spacers sandwiching a 25 μm thick platinum wire (60 μm electrode spacing, assembly for cell with μRE).

Fig. 3 shows *j-V* curves and WE vs. CE impedance spectra of these cells. All modifications were within the regular margin of variation for one set of cells. According to the increased electrode distance, the diffusion-related contribution, i.e., the Warburg parameter Z_{Ws} (from W_s), slightly increased for type C (Table 2). However, the solar cell parameters were not affected by the adjustment of the architecture (Table 2), indicating that types B and C functioned as desired and equally well to type A.

Type C cells containing a TEMPO/MBI electrolyte were then studied by μRE-assisted EIS. Typically, the impedance of a DSSC is composed of three semicircular features which are attributed to CE charge transfer superimposed to electron transport in the photoanode (high *f*), recombination at the photoanode (intermediate *f*), and diffusion of the redox mediator in the electrolyte (low *f*) [27]. Only for DSSCs with a low counter electrode impedance, the transport of electrons in the porous TiO_2 dominates at high frequencies and the CE contribution can be neglected [27]. The recorded WE vs. μRE, CE vs. μRE, and WE vs. CE spectra are shown in Fig. 4a – c, respectively.

The photoanode contribution (Fig. 4a) was fitted with the common equivalent circuit used for TiO_2-DSSCs, as the expected features originating from the transmission line model were observed at high and intermediate frequencies, corresponding to the transport of electrons in the TiO_2 (R_{tr}, high *f*) and recombination of electrons with $TEMPO^+$ (R_r, intermediate *f*), respectively. In addition, a Warburg-short element was used to account for the diffusion of the redox mediator in the electrolyte and in the porous electrode (low *f*). In the CE vs. μRE spectrum (Fig. 4b), two semicircular features were found at, however, significantly smaller absolute impedances. The intermediate-frequency feature corresponds to the reduction of $TEMPO^+$, and the feature at low frequencies is caused by the diffusion of $TEMPO^{+/0}$ in the electrolyte. Very good fits to the separated data were obtained based on the models by the respective equivalent circuits.

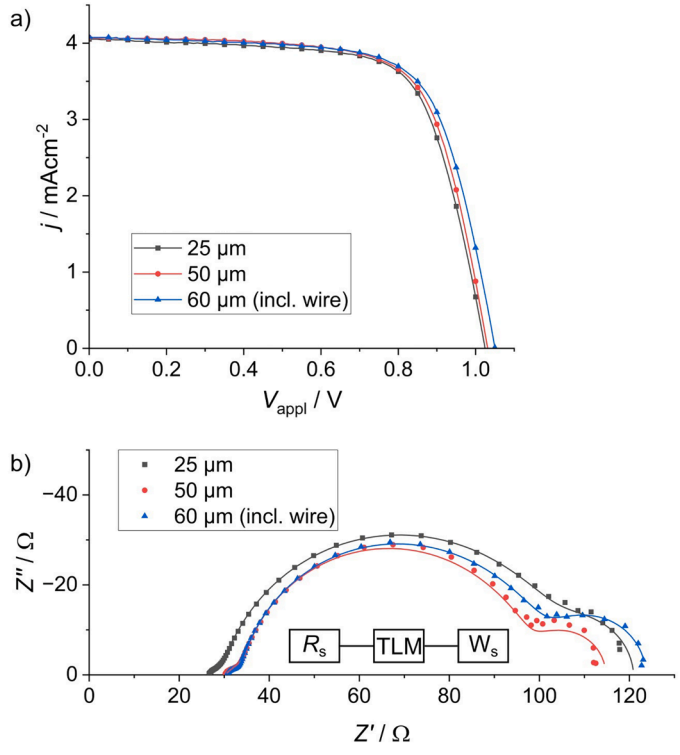

Fig. 3. Comparison of the (a) *j-V* characteristics and (b) WE vs. CE impedance spectra of TEMPO/MBI-DSSCs of different architectures A (25 μm), B (50 μm), and C (60 μm). In a), symbols are added to label the data curves. In b), symbols correspond to data points and lines represent the fits obtained with the equivalent circuit shown as inset.

Table 2
Solar cell characteristics and Warburg parameter Z_{Ws} of DSSCs in the three cell architectures leading to different separation of the photoanode and the CE.

Architecture	Z_{Ws} / Ω	j_{sc} / mA cm^{-2}	V_{oc} / V	*FF*	*PCE* / %
A, 25 μm	18.5	4.05	1.02	0.70	2.91
B, 50 μm	19.2	4.07	1.04	0.71	3.00
C, 60 μm (incl. wire)	26.1	4.07	1.05	0.70	2.99

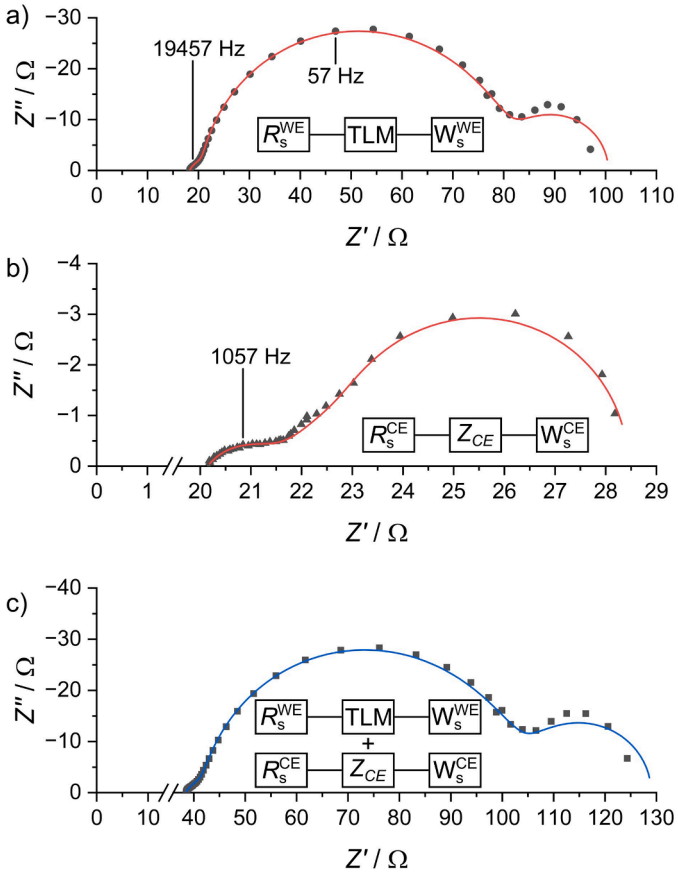

Fig. 4. (a) WE vs. μRE, (b) CE vs. μRE, and (c) reconstructed WE vs. CE impedance spectra of an aqueous 0.1 M TEMPO/MBI DSSC with a PEDOT counter electrode in the proposed architecture using a μRE in the cell. Symbols represent data points, while red lines are the fits performed with the respective equivalent circuits shown as insets. The blue line in c) shows the superposition of the fits of sub-spectra a) and b). A direct, quantitative comparison of the three spectra is provided in Fig. S2.

Fig. 4c shows the superposition of the individual WE vs. μRE and CE vs. μRE fits which perfectly describe the experimental impedance data measured between the WE and CE of the full cell. Both, the validity of the experimental approach as well as the validity of the individual components of the equivalent circuit are, thereby, proven. Hence, the full cell equivalent circuit consisted of $R_s = R_s^{WE} + R_s^{CE}$, $Z_{Ws} = Z_{Ws}^{WE} + Z_{Ws}^{CE}$, TLM (consisting of R_{tr}, R_r, C_μ and C_{BL}), and Z_{CE} (consisting of R_{CE} and C_{CE}). The strong asymmetry of the diffusion, i.e., the significantly larger diffusion resistance in the WE half-cell, is related to the slower mediator diffusion in the porous TiO_2 network of the WE, while in the CE half-cell no such porous structure is present to hinder the electrolyte diffusion.

Thus, contributions at intermediate frequencies are characteristic for both the TLM (WE) and the reduction of $TEMPO^+$ (CE). This is noteworthy, as both contributions superimpose in the typically recorded impedance spectrum between the WE and CE as seen in Fig. 4c and cannot be discussed nor optimized separately based on such routine experiments. If EIS is used to extract R_r from such full cell impedance

(WE vs. CE) as often done in literature, rather a superposition of R_r and R_{CE} is obtained which yields reasonable values of R_r only for those cases in which R_{CE} is negligibly small. As Table 3 shows, fitting the WE vs. CE spectrum yields $R_{r\,TEMPO}^{WE\ vs.\ CE} = 57.9\ \Omega$ (with a hidden contribution of R_{CE}), while the WE vs. µRE spectrum (Fig. 4a) yielded a correct value of $R_{r\,TEMPO}^{WE} = 57.3\ \Omega$. The difference can be found in the CE vs. µRE spectrum, from which $R_{CE\ (TEMPO)} = 1.32\ \Omega$ is obtained. Since the time constants are not identical, the sum of $R_{r\,TEMPO}^{WE}$ and $R_{CE\ (TEMPO)}$ is slightly larger than the value obtained from the full cell measurement. While the slight difference of $R_{r\,TEMPO}^{WE}$ and $R_{r\ TEMPO}^{WE\ vs.\ CE}$ is negligible because of a low CE impedance, it is relevant for systems with larger CE impedances as, e.g., cells using OH-TEMPO.

Since the full cell impedance (WE vs. CE) in the three-electrode setup is reconstructed from the half-cell spectra, such a spectrum was compared to a spectrum of the same cell recorded in a true two-electrode EIS arrangement. The equivalence of the two experimental approaches is seen in the results of Fig. 5, since the difference ΔZ of Z' and Z'' of these two spectra is negligibly small (< 2 Ω down to 1 Hz).

3.3. µRE-EIS with OH-TEMPO as redox electrolyte

Subsequently, DSSCs using OH-TEMPO as the redox mediator were studied by µRE-EIS and compared to the reference cells with the TEMPO/MBI electrolyte. Substituting the $TEMPO^{+/0}$ redox couple with $OH\text{-}TEMPO^{+/0}$ in otherwise identical cells resulted in a similar R_r at a lower frequency (Fig. 6a, Table 4). This corresponds to a decreased recombination rate in accordance with the higher j_{sc} and V_{oc} for cells with OH-TEMPO compared to TEMPO/MBI cells (Fig. 2a, Table 1). At the same time, $R_{CE\ (OH\text{-}TEMPO)} = 137.1\ \Omega$ was obtained from the CE vs. µRE spectrum for OH-TEMPO/MBI (Fig. 6b), corresponding to a significantly hindered reduction of $OH\text{-}TEMPO^{+}$ at the CE. This agrees well with the significantly lower fill factor in comparison to the TEMPO/MBI cells. The finding, further, is supported by the large overpotentials necessary for OH-TEMPO/MBI to draw a significant current (Fig. 2b).

In cells of 0.1 M OH-TEMPO without organic additives (Fig. 6c and d), the impedance generally showed a similar behavior as that of TEMPO/MBI cells. However, despite a comparable recombination resistance, the solar cell characteristics were clearly inferior to the TEMPO/MBI cell (Table 1). This correlates with the differences of the chemical capacitance and, correspondingly, the recombination time constants τ_r of the interfacial element of the transmission line, which were found to be smaller for OH-TEMPO ($\tau_r = 0.52$ ms) than for TEMPO ($\tau_r = 2.68$ ms). Thus, while R_r is similar for both electrolytes, the recombination process is faster for OH-TEMPO electrolytes if no additives are used.

Increasing the OH-TEMPO concentration to 1.0 M without any additives (Fig. 6e and f) resulted in Gerischer-type behavior of the photoanode, as suggested by the absence of the high-frequency feature of electron diffusion in TiO_2. Fitting yielded $R_r < R_{tr}$ [29], which indicates a dramatic loss of the generated electrons through recombination and

Table 3
Fitting parameters of the 0.1 M TEMPO/MBI cell, corresponding to the data shown in Fig. 4, including fitting results obtained from fitting the full cell impedance (Fig. 4c) with the photoanode equivalent circuit, neglecting the CE impedance.

Parameter	WE vs. µRE (photoanode)	CE vs. µRE (counter electrode)	WE + CE (superposition)	WE vs. CE (full cell fit neglecting CE impedance)
R_s / Ω	18.3	20.1	38.4	38.5
Z_{Ws} / Ω	22.5	7.0	29.5	29.5
R_r / Ω	57.3	—	57.3	57.9
τ_r / ms	2.99	—	2.99	2.97
R_{CE} / Ω	—	1.32	1.32	—
τ_{CE} / ms	—	0.17	0.17	—

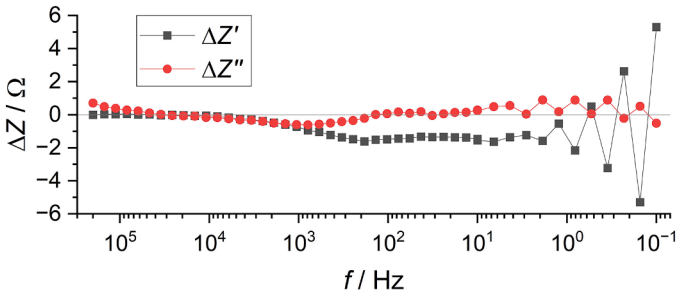

Fig. 5. Differences of the real parts ($\Delta Z'$) and the imaginary parts ($\Delta Z''$) of the total cell impedance determined either in a µRE- or in a two-electrode EIS measurement of the same 0.1 M TEMPO/MBI DSSC. Lines are added to guide the eye.

underlines the generally accepted importance of additives to suppress recombination. As also observed for the 0.1 M electrolyte without additives, the CE contribution was negligibly low. While a reasonable CE performance could be reached under these conditions, these same conditions do not allow a reasonable WE performance. To this end we could not establish a suitable cell composition yet to fully utilize the generally promising properties of OH-TEMPO.

4. Conclusions

A microscopic quasi-reference electrode was successfully incorporated in DSSCs without negatively affecting the operation of the cells. By carrying out impedance spectroscopy using the µRE, we were able to investigate the electrode kinetics of both the photoanode and the counter electrode precisely and simultaneously under operating conditions. Using this technique, a correlation of counter electrode charge transfer resistance R_{CE} and *FF* of the DSSCs was identified. Additionally, a superposition of R_{CE} and R_r was observed, suggesting that R_r obtained from the full cell impedance spectrum recorded in a regular two-electrode setup (WE vs. CE) includes contributions of R_{CE}, resulting in an over-estimation of the actual recombination resistance. It was shown that in the case of aqueous $OH\text{-}TEMPO^{+/0}$ electrolytes, MBI strongly affects the kinetics at both electrodes and while an increased R_r is beneficial, the simultaneously increased R_{CE} significantly limits the efficiency of the DSSCs. The presence of organic additives, however, proved to be necessary since low j_{sc} and V_{oc} were observed in cells without additives as a consequence of rapid recombination at the photoanode. Therefore, further optimization of the electrolyte composition and its interaction with the surfaces of WE and CE is needed to fully utilize the superior solubility and redox potential of OH-TEMPO or similar redox mediators in aqueous DSSCs. The present results indicate that localization of adsorbing additives at their target electrode is essential to avoid undesired negative impacts in other parts of the cells.

CRediT authorship contribution statement

Daniel Holzhacker: Writing – review & editing, Writing – original draft, Visualization, Methodology, Investigation, Funding acquisition, Formal analysis, Conceptualization. **Andreas Ringleb:** Formal analysis, Conceptualization. **Derck Schlettwein:** Writing – review & editing, Validation, Supervision, Resources, Project administration, Funding acquisition, Conceptualization.

Declaration of competing interest

The authors declare that they have no known competing financial interests or personal relationships that could have appeared to influence the work reported in this paper.

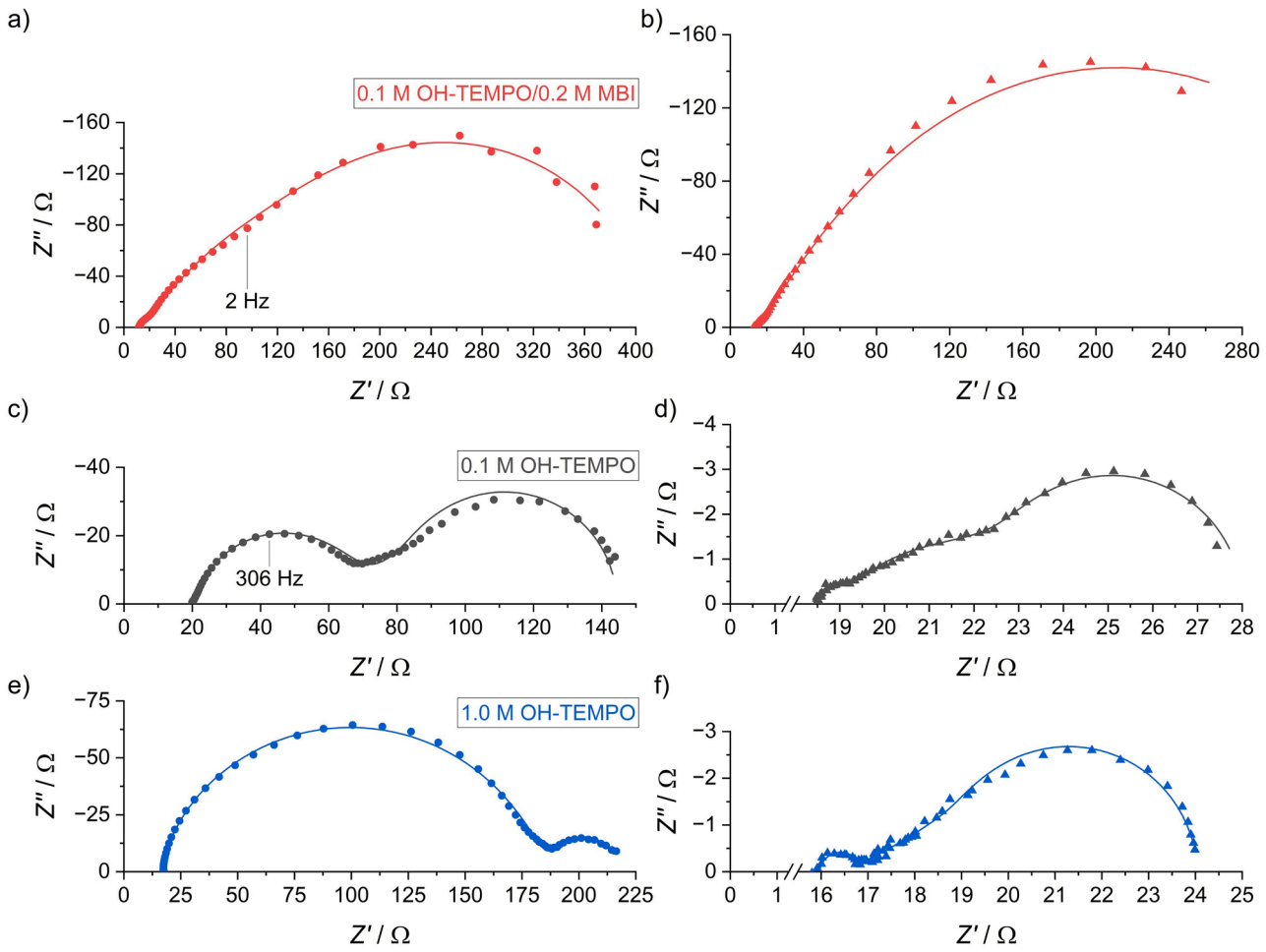

Fig. 6. Impedance spectra of OH-TEMPO cells. Circles (a, c, e) represent the WE vs. µRE spectra, while triangles (b, d, f) depict the CE vs. µRE data, and solid lines show the respective fits. A direct, quantitative comparison is shown in Figs. S3 – S5.

Table 4
Electronic transport resistance (R_{tr}), recombination resistance (R_r), and recombination time constant (τ_r) from the WE vs. µRE spectrum, and counter electrode charge transfer resistance (R_{CE}) and time constant (τ_{CE}) from the CE vs. µRE spectrum of TEMPO and OH-TEMPO DSSCs.

Electrolyte	Additive	R_{tr} / Ω	R_r / Ω	C_μ / µF	τ_r / ms	R_{CE} / Ω	τ_{CE} / ms
0.1 M TEMPO	MBI, 0.2 M	8.32	57.3	52.2	2.99	1.23	0.17
0.1 M OH-TEMPO	MBI, 0.2 M	7.17	66.0	1233	81.4	137.1	231.9
0.1 M OH-TEMPO	None	3.29	46.1	11.3	0.52	2.55	3.72
1.0 M OH-TEMPO	None	10^4 [a]	2.74	—	0.83	1.37	5.13

[a] R_{tr} was arbitrarily chosen for the 1.0 M OH-TEMPO cell due to the Gerischer-type behavior. Thus, neither R_{tr} nor R_r on their own hold physical meaning and C_μ cannot be calculated from EIS.

Data availability

Data will be made available on request.

Acknowledgements

The authors gratefully acknowledge financial support by Deutsche Forschungsgemeinschaft DFG (SCHL340/19–1, D.S.) and Deutsche Bundesstiftung Umwelt DBU (20022/040, D.H.) as well as fruitful discussions with Dr. R. Rueß (Institute of Physical Chemistry).

Supplementary materials

Supplementary material associated with this article can be found, in the online version, at doi:10.1016/j.electacta.2024.144582.

References

[1] H. Michaels, M. Rinderle, R. Freitag, I. Benesperi, T. Edvinsson, R. Socher, A. Gagliardi, M. Freitag, Dye-sensitized solar cells under ambient light powering machine learning: towards autonomous smart sensors for the internet of things, Chem. Sci. 11 (2020) 2895–2906, https://doi.org/10.1039/C9SC06145B.
[2] A. Venkateswararao, J.K. Ho, S.K. So, S.W. Liu, K.T. Wong, Device characteristics and material developments of indoor photovoltaic devices, Mater. Sci. Eng.: R: Rep. 139 (2020) 100517, https://doi.org/10.1016/j.mser.2019.100517.
[3] H. Yuan, W. Wang, Di Xu, Q. Xu, J. Xie, X. Chen, T. Zhang, C. Xiong, Y. He, Y. Zhang, Y. Liu, H. Shen, Outdoor testing and ageing of dye-sensitized solar cells for building integrated photovoltaics, Sol. Energy 165 (2018) 233–239, https://doi.org/10.1016/j.solener.2018.03.017.
[4] V. Pecunia, L.G. Occhipinti, R.L.Z. Hoye, Emerging indoor photovoltaic technologies for sustainable internet of things, Adv. Energy Mater. 11 (2021) 2100698, https://doi.org/10.1002/aenm.202100698.
[5] F. de Angelis, P. Kamat, A conversation with Michael Grätzel, ACS Energy Lett. 2 (2017) 1674–1676, https://doi.org/10.1021/acsenergylett.7b00523.
[6] F. Bella, C. Gerbaldi, C. Barolo, M. Grätzel, Aqueous dye-sensitized solar cells, Chem. Soc. Rev. 44 (2015) 3431–3473, https://doi.org/10.1039/c4cs00456f.
[7] N. Mariotti, M. Bonomo, L. Fagiolari, N. Barbero, C. Gerbaldi, F. Bella, C. Barolo, Recent advances in eco-friendly and cost-effective materials towards sustainable dye-sensitized solar cells, Green Chem. 22 (2020) 7168–7218, https://doi.org/10.1039/D0GC01148G.

[8] R.W. Ramette, R.W. Sandford, Thermodynamics of iodine solubility and triiodide ion formation in water and in deuterium oxide, J. Am. Chem. Soc. 87 (1965) 5001–5005, https://doi.org/10.1021/ja00950a005.
[9] G. Boschloo, A. Hagfeldt, Characteristics of the iodide/triiodide redox mediator in dye-sensitized solar cells, Acc. Chem. Res. 42 (2009) 1819–1826, https://doi.org/10.1021/ar900138m.
[10] M. Behl, M.D. Stout, R.A. Herbert, J.A. Dill, G.L. Baker, B.K. Hayden, J.H. Roycroft, J.R. Bucher, M.J. Hooth, Comparative toxicity and carcinogenicity of soluble and insoluble cobalt compounds, Toxicology 333 (2015) 195–205, https://doi.org/10.1016/j.tox.2015.04.008.
[11] W. Yang, M. Söderberg, A.I.K. Eriksson, G. Boschloo, Efficient aqueous dye-sensitized solar cell electrolytes based on a TEMPO/TEMPO + redox couple, RSC Adv. 5 (2015) 26706–26709, https://doi.org/10.1039/C5RA03248B.
[12] H. Ellis, R. Jiang, S. Ye, A. Hagfeldt, G. Boschloo, Development of high efficiency 100% aqueous cobalt electrolyte dye-sensitised solar cells, PCCP 18 (2016) 8419–8427, https://doi.org/10.1039/C6CP00264A.
[13] W. Zhou, W. Liu, M. Qin, Z. Chen, J. Xu, J. Cao, J. Li, Fundamental properties of TEMPO-based catholytes for aqueous redox flow batteries: effects of substituent groups and electrolytes on electrochemical properties, solubilities and battery performance, RSC Adv. 10 (2020) 21839–21844, https://doi.org/10.1039/D0RA03424J.
[14] R. Kato, F. Kato, K. Oyaizu, H. Nishide, Redox-active hydroxy-TEMPO radical immobilized in nafion layer for an aqueous electrolyte-based and dye-sensitized solar cell, Chem. Lett. 43 (2014) 480–482, https://doi.org/10.1246/cl.131120.
[15] J.L. Gómez-Cámer, P. Novák, Electrochemical impedance spectroscopy: understanding the role of the reference electrode, Electrochem. Commun. 34 (2013) 208–210, https://doi.org/10.1016/j.elecom.2013.06.016.
[16] Y. Hoshi, Y. Narita, K. Honda, T. Ohtaki, I. Shitanda, M. Itagaki, Optimization of reference electrode position in a three-electrode cell for impedance measurements in lithium-ion rechargeable battery by finite element method, J. Power Sources 288 (2015) 168–175, https://doi.org/10.1016/j.jpowsour.2015.04.065.
[17] S. Solchenbach, D. Pritzl, E.J.Y. Kong, J. Landesfeind, H.A. Gasteiger, A gold micro-reference electrode for impedance and potential measurements in lithium ion batteries, J. Electrochem. Soc. 163 (2016) A2265–A2272, https://doi.org/10.1149/2.0581610jes.
[18] J. Hertle, F. Walther, B. Mogwitz, S. Schröder, X. Wu, F.H. Richter, J. Janek, Miniaturization of reference electrodes for solid-state lithium-ion batteries, J. Electrochem. Soc. 170 (2023) 40519, https://doi.org/10.1149/1945-7111/accb6f.
[19] A.N. Jansen, D.W. Dees, D.P. Abraham, K. Amine, G.L. Henriksen, Low-temperature study of lithium-ion cells using a LiySn micro-reference electrode, J. Power Sources 174 (2007) 373–379, https://doi.org/10.1016/j.jpowsour.2007.06.235.
[20] M. Cimenti, A.C. Co, V.I. Birss, J.M. Hill, Distortions in electrochemical impedance spectroscopy measurements using 3-electrode methods in SOFC. I – Effect of cell geometry, Fuel Cells 7 (2007) 364–376, https://doi.org/10.1002/fuce.200700019.
[21] M.W. Kim, M.J. Son, H. Park, J.Y. Park, H.T. Lim, Experimental investigation of in-plane performance variation on anode supported solid oxide fuel cells using segmented cathodes and reference electrodes, Fuel Cells 20 (2020) 212–219, https://doi.org/10.1002/fuce.201900214.
[22] S.P. Jiang, Placement of reference electrode, electrolyte thickness and three-electrode cell configuration in solid oxide fuel cells: a brief review and update on experimental approach, J. Electrochem. Soc. 164 (2017) F834–F844, https://doi.org/10.1149/2.1331707jes.
[23] T. Hoshikawa, M. Yamada, R. Kikuchi, K. Eguchi, Impedance analysis for dye-sensitized solar cells with a three-electrode system, J. Electroanal. Chem. 577 (2005) 339–348, https://doi.org/10.1016/j.jelechem.2004.11.040.
[24] T. Hoshikawa, R. Kikuchi, K. Eguchi, Impedance analysis for dye-sensitized solar cells with a reference electrode, J. Electroanal. Chem. 588 (2006) 59–67, https://doi.org/10.1016/j.jelechem.2005.12.017.
[25] F. Bella, S. Galliano, G. Piana, G. Giacona, G. Viscardi, M. Grätzel, C. Barolo, C. Gerbaldi, Boosting the efficiency of aqueous solar cells: a photoelectrochemical estimation on the effectiveness of TiCl4 treatment, Electrochim. Acta 302 (2019) 31–37, https://doi.org/10.1016/j.electacta.2019.01.180.
[26] M.A. Mercadante, C.B. Kelly, J.M. Bobbitt, L.J. Tilley, N.E. Leadbeater, Synthesis of 4-acetamido-2,2,6,6-tetramethylpiperidine-1-oxoammonium tetrafluoroborate and 4-acetamido-(2,2,6,6-tetramethyl-piperidin-1-yl)oxyl and their use in oxidative reactions, Nat. Protoc. 8 (2013) 666–676, https://doi.org/10.1038/nprot.2013.028.
[27] F. Fabregat-Santiago, J. Bisquert, G. Garcia-Belmonte, G. Boschloo, A. Hagfeldt, Influence of electrolyte in transport and recombination in dye-sensitized solar cells studied by impedance spectroscopy, Sol. Energy Mater. Sol. Cells 87 (2005) 117–131, https://doi.org/10.1016/j.solmat.2004.07.017.
[28] J. Wallauer, RelaxIS user's manual, 2021.
[29] J. Bisquert, Theory of the impedance of electron diffusion and recombination in a thin layer, J. Phys. Chem. B 106 (2002) 325–333, https://doi.org/10.1021/jp011941g.